CHEMISTRY OF MATERIALS

Article

pubs.acs.org/cm

Enzymatic Synthesis and Surface Deposition of Tin Dioxide using Silicatein-α

Rute André,[†] Muhammed Nawaz Tahir,[†] Heinz Christoph C. Schröder,[‡] Werner E.G. Müller,[‡] and Wolfgang Tremel*[,†]

[†]Institut für Anorganische Chemie und Analytische Chemie, Johannes Gutenberg-Universität, Duesbergweg 10-14, D-55099 Mainz, Germany

[‡]Institut für Physiologische Chemie, Abteilung Angewandte Molekular-biologie, Johannes Gutenberg-Universität, Duesbergweg 6, D-55099 Mainz, Germany

Supporting Information

ABSTRACT: Nanostructured tin dioxide was synthesized by making use of the catalytic activity of silicatein-α. TEM, HRTEM, and XRD revealed the formation of cassiterite SnO_2. Surface bound silicatein retains its biocatalytic activity. This was demonstrated by immobilizing silicatein on glass surfaces using a histidine-tag chelating anchor. The subsequent deposition of SnO_2 on glass was monitored by quartz crystal microbalance (QCM) measurements and scanning electron microscopy (SEM). This new aspect of silicatein activity toward the formation of metal oxides other than SiO_2, TiO_2, and $BaTiO_3$ opens up new vistas in composite material synthesis.

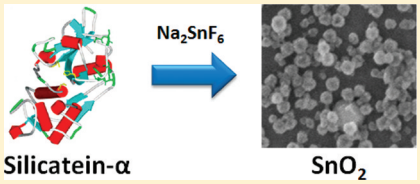

KEYWORDS: *silicatein, tin oxide, biomimetic, nanoparticles*

INTRODUCTION

In biological systems such as diatoms and sponges, the formation of solid silica structures with precisely controlled morphologies is directed by proteins and polysaccharides and occurs in aqueous media at neutral pH. Typical examples are marine sponges or diatoms where silicification is thought to occur at pH values of ~5−6.[1,2] The control over mineralization achieved in biological systems has been an inspiration for the development of new synthetic routes to materials with technological interest.[3] Biological organisms are able to synthesize a myriad of inorganic materials (calcium carbonate, calcium phosphate, silica, iron oxide, etc.) using simple precursors under mild reaction conditions, usually at ambient temperature and almost neutral pH, resulting in highly complex structures with several levels of hierarchy from the nano to the macro level.[4]

Mostly, these mineralized materials are formed either by controlled condensation in specific compartments, e.g., by regulating the concentration of the inorganic precursors or by enzymatic catalysis. In the case of demosponges like *Tethya aurentia* or *Suberites domuncula*, the inorganic skeleton composed of silica spicules is formed by the catalytic activity of one special class of proteins, the silicateins.[5,6] These proteins have proven very versatile: besides the formation of silica and polysilsesquioxanes,[7−9] they can also catalyze the formation of TiO_2,[10] ZrO_2,[11] $CaTiO_3$,[12] and $GaOH/Ga_2O_3$.[13] The slow hydrolysis and polycondensation in these syntheses were derived from a mechanism underlying biosilicification,[7,8] which was confirmed through cloning, site-directed mutagenesis and detailed biochemical investigations.[14]

The broad variety of "synthetic biomaterials" that can be obtained with silicatein indicates that this protein has a very flexible active site. Therefore a very general mechanism can be assumed to underly its catalytic activity. Furthermore, the materials catalyzed by silicatein (native and recombinant) often exhibit crystalline polymorphs that are uncommon for low temperature syntheses (e.g., anatase-type TiO_2,[15,16] cubic ZrO_2,[10] or γ-Ga_2O_3[13]) and that are usually only obtained at high temperatures or under extreme pH conditions.[17]

The mechanism underlying enzyme-mediated biosilicif ication was translated into a bioinspired approach (i) by using the intact axial protein filament from *T. aurantia* or their constitutional monomers obtained by disaggregation of the filaments,[18] (ii) or those produced from recombinant DNA templates cloned in bacteria.[7,19] (iii) The corresponding recombinant proteins could be surface bound to produce thin films of silica,[20] titania,[16] or zirconia.[10] (iv) Finally, kinetically controlled catalytic hydrolysis and polycondensation could be achieved through development of synthetic analogs of the enzyme responsible for biosilicification.[9,21]

The latter process uses vapor diffusion of a hydrolytic catalyst into the solution of a molecular precursor to establish temporal and spatial vectorial gradients of catalyst concentration for the kinetically slow hydrolysis of precursor monomers at room temperature and ambient pressure. Functionalized gold nanoparticles mimic catalytic activity of a polysiloxane-synthesizing enzyme. We recently found that core−shell TiO_2@SiO_2 and

Received: July 11, 2011
Revised: November 4, 2011
Published: November 4, 2011

TiO_2@ZrO_2 nanofibers can be obtained via grafting of silicatein-α onto a TiO_2 nanowire backbone followed by a coassembly of "sticky" protein, silintaphin-1, through its specifically interacting domains.[22] This mechanism can be harnessed for nanostructural control of patterned biosilica-based biomaterials. To test the possibility that the catalytic potential of silicatein can be used for building up complex functional inorganic/organic hybrid materials by successive hydrolysis and condensation reactions, we examined the formation of nanostructured crystalline tin dioxide using surface-bound silicatein in aqueous solution. Tin dioxide is a well-known wide band gap semiconductor material that combines high conductivity with high optical transparency in the visible range,[23] making it an important component for optoelectronic applications. These properties have been already demonstrated in applications as transparent conducting oxides in electrodes for solar cells[24] or lithium-ion batteries.[25] Tin dioxide has also been used as a heterogeneous oxidation catalyst[26] or as a solid-state gas sensor.[27]

The efficiency of these materials is closely related to their nanoscopic properties, the surface to volume ratio being of crucial importance. Furthermore semiconductor nanocrystals are attractive candidates for nanoscale devices due to their enhanced physicochemical properties compared with the bulk materials.[28] All these properties have raised a special interest in the synthesis of nanostructured tin dioxide in recent years. Several different morphologies have been achieved like nanodiscs,[29] nanobelts,[30] nanorods,[31] among others, usually applying vapor deposition,[32] solvothermal,[33] or microwave[34] routes. Hollow SnO_2 nanoparticles were prepared by a template-free hydrothermal route.[35] Also the formation of tin dioxide using amino acids via hydrothermal route or polypeptides at room temperature (reaction times up to 2 weeks) has been reported recently.[36] In all cases, the synthetic routes either demand for harsh conditions though with good structural control, whereas milder conditions lead structures with less morphological and structural control.

A crucial point for the formation of metal oxides is the versatility of the synthetic route, as they have a broad field of application, either used as thin films or as free-standing nanoparticles. In this contribution we show that silicatein is able to produce not only nanostructured SnO_2 dispersed in solution but also when immobilized on surfaces (glass slide), thereby providing flexible and mild biomimetic pathways for the fabrication of SnO_2-based materials with potential applications in catalysis or optoelectronics.

EXPERIMENTAL SECTION

Methods and Materials. Sodium hexafluorostannate (Na_2SnF_6, ABCR, 99%), Tris buffered saline (TBS, Sigma-aldrich), bovine serum albumin (BSA) blocking solution (Carl Roth), Cy3-conjugated goat antirabbit antibody (Dianova), 3-(2,3-epoxypropoxy)propyltrimethoxysilane (Sigma-Aldrich) and N,N-Bis(carboxymethyl)-L-lysine hydrate (Sigma-Aldrich) were purchased and used as received without further purification. Solvents, acids, and bases, such as ethanol, dichloromethane, toluene, HCl, HNO_3, and NaOH, were purchased technical grade and used as received.

Synthesis. *Silicatein-α Production.* Recombinant silicatein-α was prepared as described before.[6,37] Silicatein was obtained and used in TBS (Tris buffer saline, pH 7.4) as working buffer.

Protein-Assisted Synthesis of Tin Oxide (SnO_2). For SnO_2 biosynthesis, 1 mL of 5 mM solution of sodium hexafluorostannate (Na_2SnF_6) in TBS buffer, pH 7.4 was added to 500 μL of a solution of recombinant silicatein-α (50 mg/mL) in TBS buffer pH 7.4, and kept under agitation at room temperature for 4 h. The white precipitate formed was washed several times with Milli-Q water and ethanol and dried in an oven at 60 °C overnight. The product was used as prepared or after annealing at 200 °C under air, for 2 h. As control experiments the same concentration of Na_2SnF_6 was incubated only in TBS buffer at pH 7.4, or with denaturated silicatein-α under the same conditions. For protein denaturation, a heat treatment at 95 °C for 10 min was performed.

Immunostaing and Light Microscope Imaging. Specific anti-silicatein antibodies were prepared as described before.[6] The presence of silicatein was monitored by incubating the as-synthesized tin-oxide with primary antisilicatein (produced in mouse) polyclonal antibody (1:2000 dilution), in a 5% blocking solution (BSA) for 2 h at room temperature. The sample was washed several times using TBS buffer (pH 7.4) for 5 min followed by the secondary antibody, antimouse Cy3 labeled (1:2000 dilution), incubation in 5% blocking solution (BSA) for 3 h at room temperature, and then washed with TBS. The as-synthesized product was washed only with buffer (TBS, pH 7.4) before performing the immunostaing in order to maintain the included protein in the structures. As control, annealed SnO_2 samples were used, where no protein was expected to be found due to the heat treatment. For immunostaining in functionalized glass surfaces the same procedure was used. The fluorescence analysis was performed with an Olympus AHBT3 light microscope, together with an AH3-RFC-reflected light fluorescence attachment at the emission wavelength of 580 and 499 nm.

Glass Slide Functionalization with Recombinant Silicatein-α. Glass slides with an average 1 cm ×1 cm in dimension were cleaned with piranha solution (H_2SO_4/H_2O_2, 1:3) for 30 min at room temperature. The slides were rinsed several times with distilled water and dried under a stream of nitrogen. For the functionalization of the glass slides with the histidine-tagged silicatein a modified procedure by Chevalier et al.[38] was used. Briefly, the glass slides where added to a solution of 3-(2,3-epoxypropoxy)propyltrimethoxysilane (2% in toluene) and kept overnight at room temperature, under an argon atmosphere. After rinsing with dry toluene and 10 mM carbonate buffer pH 10, the glass supports were incubated with 20 mM N,N-bis(carboxymethyl)-L-lysine hydrate (in carbonate buffer, 10 mM pH 10) overnight at room temperature. Once again the surfaces were rinsed with carbonate buffer and then submerged in a 100 mM $NiSO_4$ solution for 30 min. The surfaces were washed with a 150 mM solution of NaCl, and incubated with a 100 μg/mL solution of silicatein-α in TBS buffer, pH 7.4, for 2 h. To remove unbound protein, we washed the surfaces with TBS buffer several times.

Characterization. *(High Resolution) Transmission Electron Microscopy (HR)TEM.* Characterization and morphology analysis of the samples was carried out using transmission electron microscopy (TEM) using a Philips 420 instrument with an acceleration voltage of 120 kV or for high resolution TEM, a Philips TECNAI F30 electron microscope (field-emission gun, 300 kV extraction voltage).

Scanning Electron Microscopy and Energy-Dispersive X-ray Spectroscopy (SEM-EDX). The samples were mounted on aluminum stubs covered with adhesive carbon (Leit-Tabs No.: G 3347 [Plano, Wetzlar; Germany]) and analyzed by scanning electron microscopy using a Nova 600 NanoLab SEM equipped with an EDAX Division EDX analyzer.

X-ray Powder Diffraction. The sample was analyzed by X-ray powder diffraction (XRD) in $\theta/2\theta$ reflection geometry using a Siemens D8 power diffractometer equipped with a position sensitive detector. The data were collected using Cu−Kα radiation at an operating potential of 40 kV and a current of 40 mA, and analyzed using the EVA software.[39]

UV−Vis Spectroscopy. The SnO_2 powders were dispersed in Milli-Q water and slightly sonicated prior to transfer to quartz cuvettes. Glass slides were washed with Milli-Q water and dried at 60 °C for 5 h prior to measure. The samples were then measured at room temperature and in the range between 200 and 800 nm using a Varian Cary 5G UV/vis spectrophotometer.

Quartz Crystal Microbalance (QCM). Measurements were performed on a Q-sense D300 instrument using the axial flow chamber

dx.doi.org/10.1021/cm201977c | Chem.Mater. 2011, 23, 5358−5365

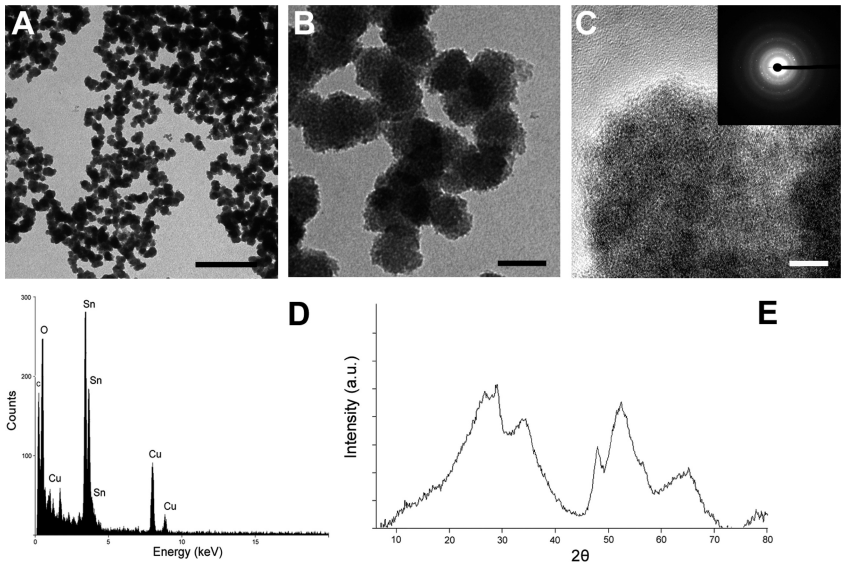

Figure 1. SnO_2 obtained by silicatein-mediated synthesis. (A, B) TEM micrographs of the as-synthesized product. (C) HRTEM micrograph of the as-synthesized product with electron diffraction pattern in the inset; (D) EDX and (E) XRD of the as-synthesized product.

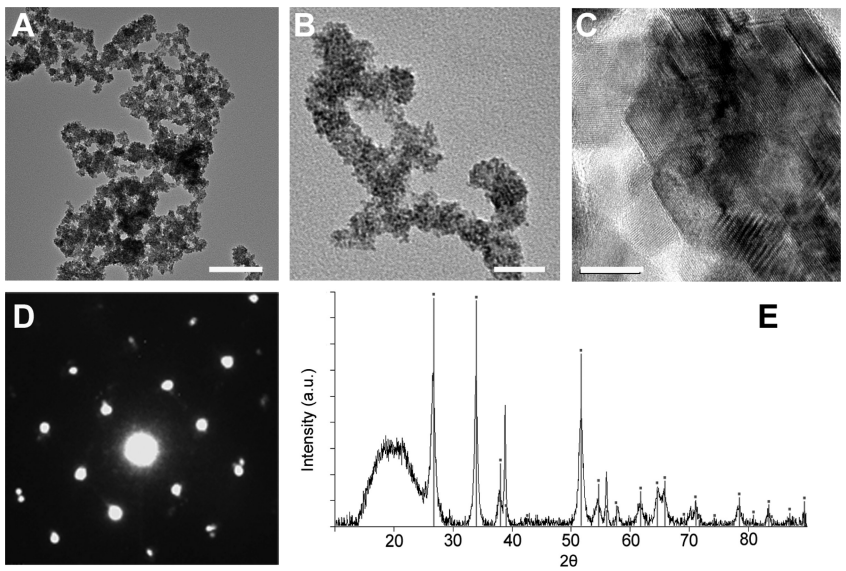

Figure 2. Characterization of SnO_2 synthesized using silicatein as hydrolytic catalyst, after annealing at 200 °C. (A, B) TEM micrographs of the annealed product. (C) HRTEM of the annealed product. (D) Electron diffraction referring to the spot in C. (E) XRD pattern of the annealed product and calculated powder pattern (gray vertical lines) for cassiterite (PDF 41−1445). Scale bars: 100, 20, and 10 nm, respectively.

and a quartz crystal sensor with the gold electrode coated with 50 nm of silicon dioxide (Q-sense QSX 303, AT-cut, 5 MHz). The silicon dioxide surface was functionalized ex situ with silicatein, using the procedure described above for the glass slides. For the measurement, the functionalized crystal was placed in the sensor chamber with TBS buffer (pH 7.4) until a stable frequency baseline established, and then the precursor solution (5 mM Na_2SnF_6) was introduced. The resonant frequency and dissipation were measured at intervals of 40 ms (25 °C for 30 min), after which the sensor was washed with buffer to eliminate possible adsorbed precursor. The changes in mass were calculated using Sauerbrey equation[40]

$$\Delta m = -17.7 \text{ ng Hz}^1 \text{ cm}^{-2} \Delta f / n$$

Where m is de adsorbed mass, f is the frequency, and n is the overtone number.

RESULTS AND DISCUSSION

The synthesis of SnO_2 nanostructures was achieved by incubating 5 mM of Na_2SnF_6 precursor with recombinant silicatein-α (50 μg/mL) in TBS (Tris buffer saline) buffer pH 7.4 under agitation at room temperature. After approximately 4 h a visible white precipitate was formed. Controls using either only TBS buffer or the denaturated protein showed no precipitate formation or any other reaction product (see the Supporting Information, Figure S1). After extensive washing with water and ethanol, to remove unbound protein and buffer salts, the precipitate was dried and characterized by transmission electron microscopy (TEM). The overall sphere like morphology of the as-synthesized product can be seen in Figure 1A. The spherical agglomerates have an average size of 50 nm. Silicatein typically assembles in a fractal manner

dx.doi.org/10.1021/cm201977c | Chem.Mater. 2011, 23, 5358−5365

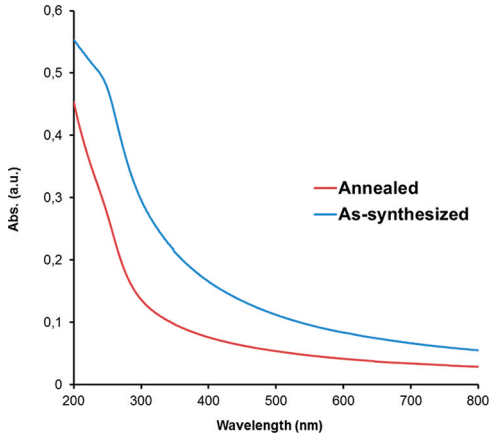

Figure 3. UV–vis spectra of SnO_2 synthesized using silicatein as hydrolytic catalyst. Blue line, spectrum of the as-synthesized product. Red line, spectrum of the annealed product (200 °C).

forming agglomerates. When incubated with silica precursors similar structures are obtained.[18] The morphology of the product in Figure 1 is assumed to arise from a templating effect of the protein agglomerates. Zooming into the sample shows that the sphere-like agglomerates are composed of smaller particles appearing as amorphous/nanocrystalline material (Figure 1B and C). TEM and HRTEM reveal that the product is made up of amorphous as well as small crystal domains (between 2 and 5 nm). EDX of the sample (Figure 1D) shows only the presence of carbon, tin and oxygen. The copper signal arises from the grids used for the sample preparation. In the crystal domains, a *d* spacing of 3.3 Å was obtained for the lattice fringes, which is a good match to the (110) planes of SnO_2. Electron diffraction on the sample (inset in Figure 1C) supports the presence of some crystal domains.

X-ray diffractometry was used to determine the overall composition and structure of the products. It requires the availability of material in sufficient amount and purity. X-ray diffraction patterns of all samples (see Figure 1E) indicate the presence of SnO_2 (cassiterite, PDF 41–1445) independent of the choice of reaction parameters. The reflection broadening due to particle size effects prevents a quantitative determination of the pattern using Rietveld methods. However, the presence of few very broad reflections in Figure 1E indicates the formation of a product composed of mainly

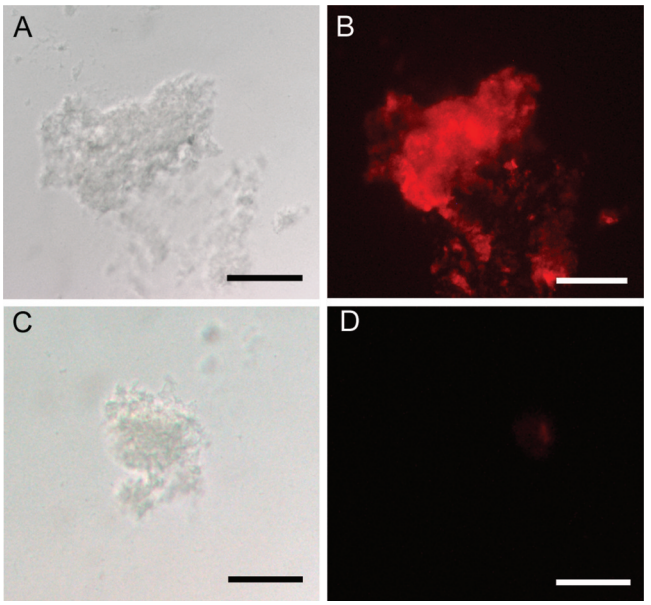

Figure 4. Light and fluorescence optical micrographs of the immunostaining against silicatein for SnO_2 formed in the presence of the protein. (A) Light and (B) fluorescence micrographs of immunostaining on as-synthesized product indicating the presence of silicatein. (C) Light and fluorescence micrographs of immunostaining on annealed product where no specific binding was detected. Scale bar: 5 μm in all images.

amorphous and/or small crystallites. The position of the main reflections is compatible with the presence of tin dioxide.

Heat treatment of the sample (200 °C for 2 h) was used to further characterize the product and probe any possible phase transformation. TEM images in Figure 2A and B reveal a decrease in aggregate size to about 20 nm while maintaining the small crystallite size. HRTEM (Figure 2C) shows an increase in the crystal domain size with values ranging from 5 to 10 nm. Lattice fringe measurements still show an average value of 3.3 Å for the (110) plane of tin dioxide. For the larger particles shown in Figure 2C, the distances between two adjacent planes are 1.6, 2.4, and 3.3 Å, corresponding to the (220), (110), and (200) planes of cassiterite (Figure 2D). The powder X-ray diffraction pattern in Figure 2E shows sharpened reflections whose positions and relative intensities match well with

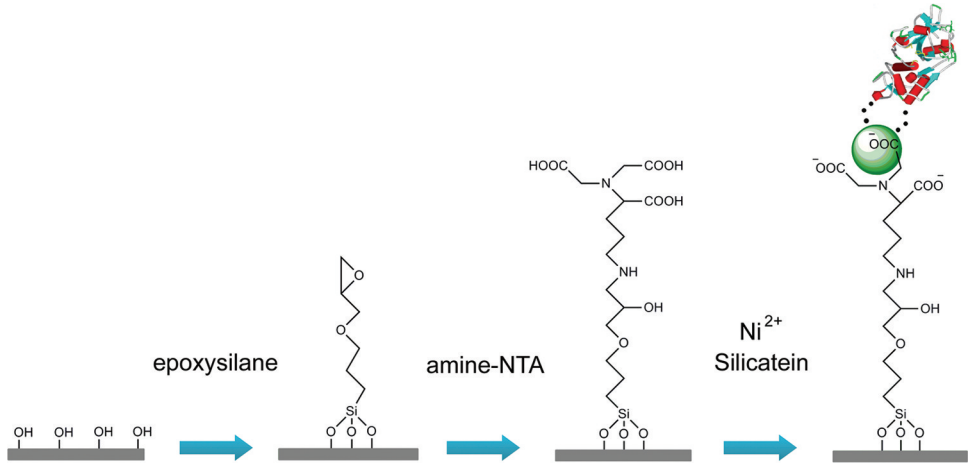

Figure 5. Scheme illustrating the steps for glass slide functionalization with histidine tagged silicatein (illustrations not to scale).

dx.doi.org/10.1021/cm201977c | *Chem.Mater.* 2011, 23, 5358–5365

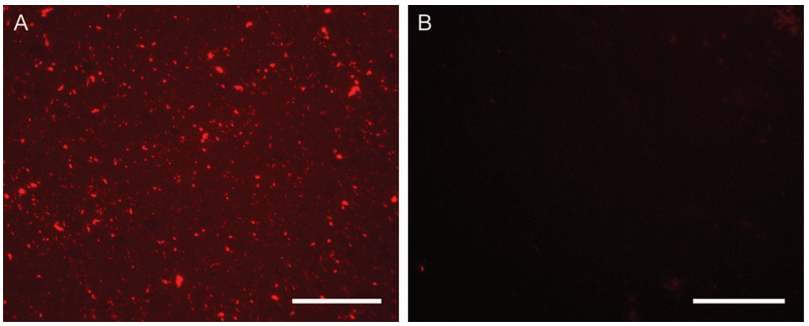

Figure 6. Fluorescence microscopy images showing the immunostaing against silicatein on (A) amine NTA/silicatein functionalized glass surfaces and (B) on nonfunctionalized glass surface (direct incubation with silicatein) as control. Scale bars: 5 μm.

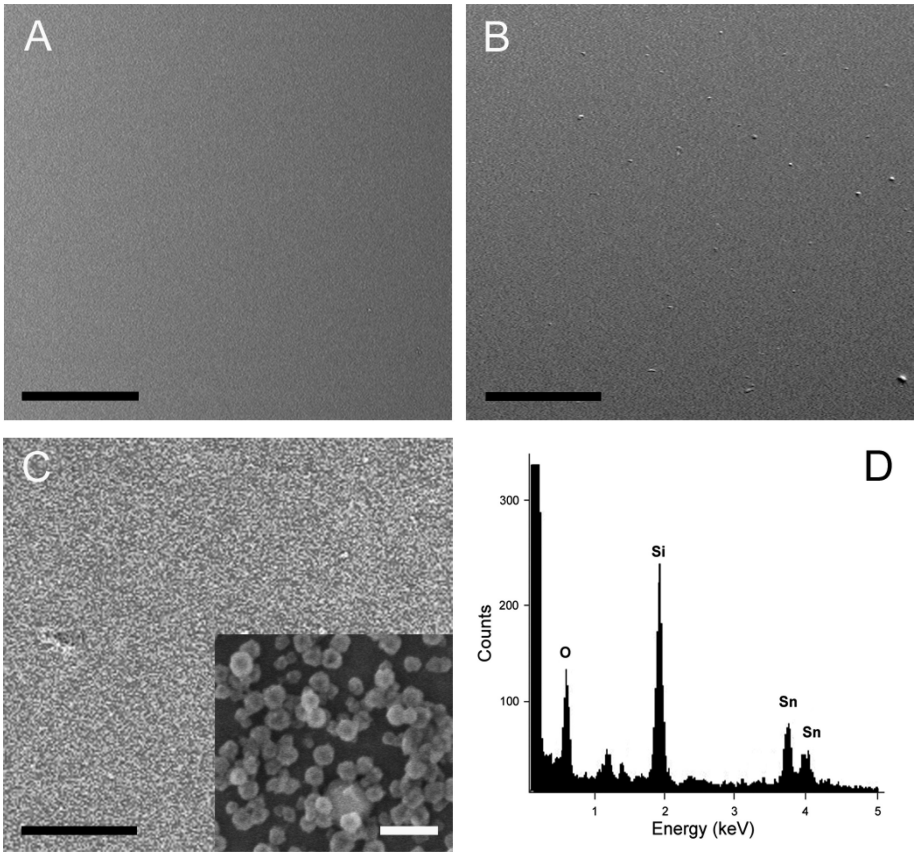

Figure 7. SEM images of (A) a bare glass slide, (B) ,onfunctionalized glass slide after incubation with the SnO_2 precursor, (C) NTA/silicatein functionalized glass slide after incubation with the SnO_2 precursor. Inset: High-resolution of where the typical spherelike shapes are observed (scale bar: 100 nm). (D) SEM-EDX corresponding to the spot in C. Scale bars: 5 μm.

expected pattern for cassiterite (PDF 41−1445, gray vertical lines in Figure 2E) as in the freshly synthesized product.

The typical plasmon band of SnO_2 was identified in both samples, as-synthesized and annealed, at around 280 nm as can be inferred from the UV−vis spectra in Figure 3. The absorption band edge for SnO_2 was reported to be around 300 nm.[41] In the prepared samples the band edge is blue-shifted to 280 nm which indicates, in agreement with the small particle size, the presence of a quantum size effect. For both, the as-synthesized and the annealed sample, the spectra are similar, showing that the annealing process does not change the intrinsic properties of the material.

Monoclonal antibodies directed against recombinant silicatein-α were used to demonstrate the binding of silicatein between the individual SnO_2 domains by CLSM through the positive cross-reaction between the SnO_2 particles and the polyclonal antibodies raised against silicatein-α (PoAb-aSILIC, Figure 4B).[42] To avoid protein damage, the product was washed with buffer several times to remove unbound protein, maintaining in that way the included protein responsible for the SnO_2 precipitation. The fluorescence microscope image in Figure 4B indicates that silicatein is distributed and included in the as-synthesized tin-oxide sample. No fluorescence was observed in the control experiments (Figure 4D). As a control (to rule out unspecific interaction of the antibodies with the material), the annealed SnO_2 samples were submitted to immunostaining, and no fluorescence could be detected (Figure 4C, D).

dx.doi.org/10.1021/cm201977c | *Chem.Mater.* 2011, 23, 5358−5365

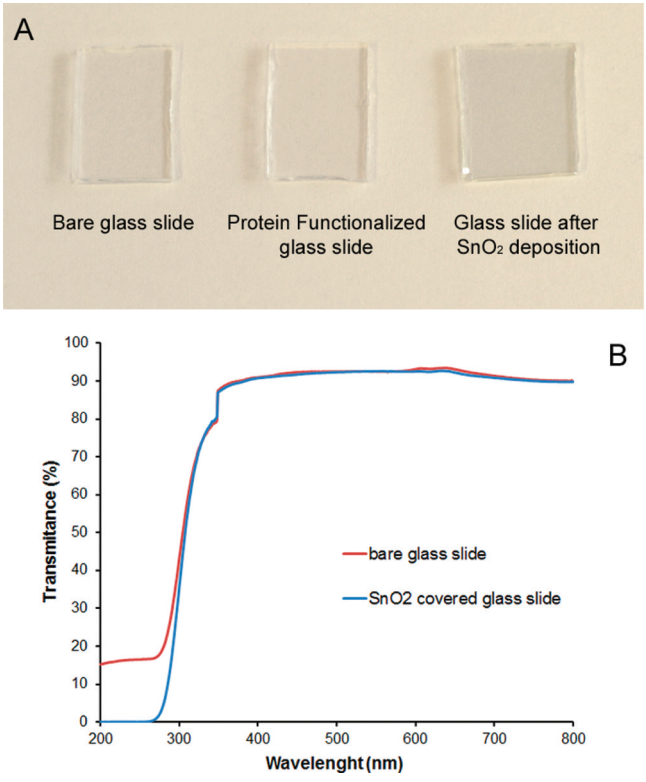

Figure 8. Optical images of glass slides covered SnO_2 mediated by silicatein. (A) Glass slides before and after SnO_2 deposition. Almost no color change was detected after functionalization with protein and deposition of SnO_2. (B) Transmittance in the UV−vis range of the bare glass slides (red) and the SnO_2 covered glass slides (blue).

When the reaction was performed under the same conditions but with denaturated silicatein-α, no precipitate was observed (see the Supporting Information, Figure S1). This indicates that the catalytic activity of silicatein for the formation of SnO_2 is dependent on the three-dimensional integrity of the protein, and that silicatein is occluded in the formed structures.

Regarding the mechanism of formation of SnO_2 in the presence of silicatein, we can infer that the protein plays an active role in the hydrolysis of the precursor, which otherwise is stable in aqueous solution at room temperature (as shown in Figure S1 in the Supporting Information). Attempts to determine the reaction intermediates by ^{119}Sn or ^{19}F NMR or FTIR were unsuccessful, most likely because the concentration of the protein and the precursors in solution were close to the detection limit of those methods.

Therefore, we propose that silicatein catalyzes the hydrolysis of the hexafluorostannate, which condensates in a subsequent step to form SnO_2 crystallites. Because of the lower Pearson hardness of Sn compared to Si and the resulting lower degree of hydration small crystallites (rather than amorphous and partially hydrated material) are formed. The nucleating SnO_2 nanocrystals are stabilized by surface binding of silicatein. Upon aggregation of these nanocrystals, domain crystals[43] with nanometer-sized domains are formed. These results indicate that silicatein has not only a catalytic but also a potential templating and constraining effect on the formation of SnO_2.

Tin dioxide is a well-studied and widely used semiconductor. Therefore, facile and sustainable synthetic routes are necessary which can be expected to have a widespread application. As recombinant silicatein-α promotes the formation of SnO_2 at neutral pH, in aqueous media and at room temperature in an economic and simple fashion, we have studied the deposition of SnO_2 mediated by silicatein on glass surfaces.

Self-assembled monolayers (SAM) of alkanethiol derivatives on metal electrodes provide numerous possibilities for immobilizing proteins.[44] Glass surfaces were chosen as a common substrate for the deposition of tin dioxide and derived composite materials that form the basis for transparent semiconductor surfaces which have further applications in solar cell assembly or intelligent glass displays. Hence, recombinant silicatein was immobilized on glass surfaces by complexation with a histidine tag, Ni^{2+} and nitrilotriacetic acid (NTA) as described elsewhere.[45] In short, the glass slides were silanized with 3-(2,3-epoxypropoxy) propyltrimethoxysilane which was further functionalized with amine terminated nitrilotriacetic acid. This allowed, after incubation with Ni^{2+}, the immobilization of histidine-tagged silicatein on the surface, as illustrated in Figure 5.

The presence of silicatein on glass surfaces was assessed by immunostaining with specific antisilicatein antibodies, after blocking the surface with BSA, to avoid any unspecific interaction of the antibodies with the surface. As seen in Figure 6A, a complete coverage of the surface was achieved. Bare glass surfaces (nonfunctionalized with NTA ligand) were also incubated with protein, where no binding was observed (Figure 6B). Thus the functionalization method using a NTA linker on the glass surface proved to be efficient for further functionalization with the recombinant histidine-tagged silicatein.

To obtain a tin dioxide coating on the functionalized glass surface, incubation with Na_2SnF_6 (5 mM, TBS buffer pH 7.4) was performed for 4 h. Subsequently, the surface was washed extensively with water and ethanol and dried at 60 °C for 5 h. As a control, nonfunctionalized surfaces were incubated with the tin dioxide precursor under the same conditions.

The morphology of the surfaces with and without SnO_2 was investigated using SEM. Figure 7A shows the bare glass slide before functionalization. The control experiment (nonfunctionalized glass) does not show any significant deposition (Figure 7B). The surfaces incubated with the tin dioxide precursor in the presence of silicatein (Figure 7C) show a substantial homogeneous surface deposition, where the material has a similar appearance (inset Figure 7C) as SnO_2 synthesized by silicatein in solution (Figure 1A). Elemental analysis with EDX clearly shows the presence of Sn, O and Si (from the glass) thereby demonstrating that tin dioxide is present on the glass surface (Figure 7D).

The color of the glass slides did not change significantly after tin dioxide deposition, and the transparency in the visible light was maintained (Figure 8A), where, at the macroscopic level, both functionalized and nonfunctionalized surfaces look virtually identical. The transmittance of the surface in the UV range is similar for the bare and the SnO_2 covered glass slides (Figure 8B); only a slight decrease in transmittance is present between 200 and 250 nm for the SnO_2-coated glass.

The deposition profile of tin oxide on functionalized glass surfaces was monitored using a quartz crystal microbalance (QCM). With this method, it is possible to obtain

dx.doi.org/10.1021/cm201977c | Chem.Mater. 2011, 23, 5358–5365

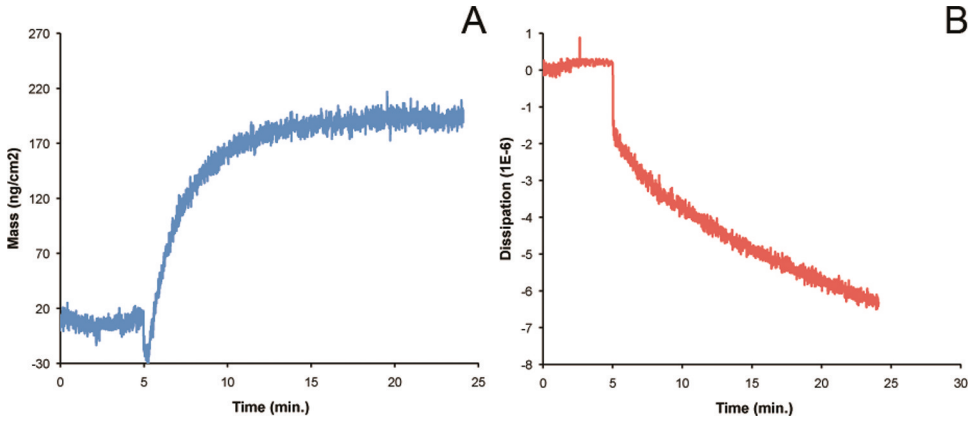

Figure 9. QCM measurement of tin oxide deposition on silicatein-functionalized quartz sensors. Injection of the tin oxide precursor was made after 5 min as indicated by the sudden change in the mass (frequency) and dissipation values. (A) Evolution of mass deposited over time and (B) change in dissipation as a function of the reaction time.

information on the mass deposited on the surface and on the elasticity of the deposited films. Silicon dioxide covered QCM sensors were used, which were functionalized with silicatein in the same manner as the previously shown glass slides. After addition of the precursor solution, the mass change (Δm) was monitored continuously with time. (Figure 9A) With the addition of the precursor solution the growth rate rapidly increases during the first 5 min and then it decreases during the remaining reaction time, possibly due to enzyme saturation. A control experiment on a non-functionalized QCM sensor, using the same precursor concentration showed small or no deposition during the same reaction time (see the Supporting Information, Figure S2). Hence it can be concluded that the mass deposition is exclusively due to the presence of silicatein-α. Furthermore, the dissipation data (Figure 9B) indicates the formation of a rigid film (decrease in dissipation over time) which is as expected for a mineralized surface.

SEM pictures were taken from the sensor after the reaction time (see the Supporting Information, Figure S3A) were the presence of similar structures as for the SnO2 deposition in the glass slides (Figure 7) is clearly visible. In the control experiment no significant deposition was observed (Supporting Information, Figure S3B).

CONCLUSIONS AND OUTLOOK

In summary, we were able to demonstrate that recombinant silicatein-α can mediate the formation of nanostructured crystalline SnO_2 under mild conditions, i.e., at room temperature and neutral pH, in a buffered system. Silicatein can be assumed to have a catalytic effect on the synthesis of tin dioxide through the enhanced hydrolysis of the precursor compounds. The freshly synthesized product contains spherical agglomerates of smaller particles with crystalline domains of cassiterite. After the product was annealed at 200 °C, the SnO_2 cassiterite phase was maintained. The typical surface plasmon absorption band for SnO_2 was identified by optical spectroscopy. Silicatein has a constraining effect on the particle size due do the agglomeration of the protein on the newly formed crystals. The SnO_2 product nanoparticles are stabilized by surface binding of silicatein through its functional (amino and/or carboxylate) groups, as shown by fluorescence microscopy using a fluorophore attached to silicatein by specific antigen−antibody interactions.

In addition, recombinant silicatein-α was immobilized on glass slides using epoxysilane/NTA ligands. After incubation with a tin oxide precursor, a layer of SnO_2 was successfully synthesized. The glass slides after the catalytic deposition of tin oxide remain colorless and transparent in the UV range, thus indicating the potential application of this simple deposition method in the development of new composite materials with technological interest, for example, in production of transparent conductive oxides.

ASSOCIATED CONTENT

Supporting Information

(1) Optical micrographs of as-synthesized product and controls with denaturated protein, (2) QCM analysis of control experiments, (3) SEM of QCM sensors after tin oxide deposition. This material is available free of charge via the Internet at http://pubs.acs.org/.

AUTHOR INFORMATION

Corresponding Author

*Phone: +49 6131 392-5135. Fax: +49 6131 392-5605. E-mail: tremel@uni-mainz.de.

ACKNOWLEDGMENTS

This work was supported by the Deutsche Forschungsgemeinschaft (DFG) within the priority program 1420 "Biomimetic Materials Research and the BMBF center of Excellence BIOTEC Marin. The authors acknowledge support for the Electron Microscopy Center in Mainz (EZMZ) from the Center for Complex Matter (COMATT).

REFERENCES

(1) *Handbook of Biomineralization*, 1st ed.; Bäuerlein, E., Behrens, P., Epple, M., Eds.; Wiley-VCH: Weinheim, Germany, 2007.
(2) Nassif, N.; Livage, J. *Chem. Soc. Rev.* **2011**, *40*, 849−859.
(3) Mann, S.; Archibald, D. D.; Didymus, J. M.; Douglas, T.; Heywood, B. R.; Meldrum, F. C.; Reeves, N. J. *Science* **1993**, *261*, 1286−1292.
(4) (a) Lakes, R. *Nature* **1993**, *361*, 511−515. (b) Ozin, G. A. *Acc. Chem. Res.* **1997**, *30*, 17−27. (c) Douglas, T. *Science* **2003**, *299*, 1192−1193.
(5) Shimizu, K.; Cha, J.; Stucky, G. D.; Morse, D. E. *Proc. Natl. Acad. Sci. U.S.A.* **1998**, *95*, 6234−6238. (b) Brutchey, R. L.; Morse, D. E. *Chem. Rev.* **2008**, *108*, 4915−4934. (c) Schröder, H. C.; Wang, X.; Tremel, W.; Ushijima, H.; Müller, W. E. G. *Nat. Prod. Rep.* **2008**, *25*,

455−474. (d) Schröder, H. C.; Wiens, M.; Schlossmacher, U.; Brandt, D.; Müller, W. E. G. *Silicon* **2010**, 1−9, ; DOI: 10.1007/s12633-010-9057-4.
(6) (a) Krasko, A.; Batel, R.; Schröder, H. C.; Müller, I. M.; Müller, W. E. G. *Eur. J. Biochem.* **2000**, *267*, 4878−4887.
(7) Cha, J. N.; Shimizu, K.; Zhou, Y.; Christiansen, S. C.; Chmelka, B. F.; Stucky, G. D.; Morse, D. E. *Proc. Natl. Acad. Sci.* **1999**, *96*, 361−365.
(8) Zhou, Y.; Shimizu, K.; Cha, J. N.; Stucky, G. D.; Morse, D. E. *Angew. Chem., Int. Ed.* **1999**, *38*, 779−782.
(9) Wolf, S. E.; Schloßmacher, U.; Pietuch, A.; Mathiasch, B.; Schröder, H. C.; Müller, W. E. G.; Tremel, W. *Dalton Trans.* **2009**, *39*, 9245−9249.
(10) Sumerel, J. L.; Yang, W.; Kisailus, D.; Weaver, J.; Choi, J. H.; Morse, D. E. *Chem. Mater.* **2003**, *15*, 4804−4809.
(11) Tahir, M. N.; Théato, P.; Müller, W. E. G.; Schröder, H. C.; Boreijko, A.; Faiß, S.; Janshoff, A.; Huth, J.; Tremel, W. *Chem. Commun.* **2005**, *28*, 5533−5535.
(12) Ould-Ely, T.; Luger, M.; Kaplan-Reinig, L.; Niesz, K.; Doherty, M.; Morse, D. E. *Nature Protocols* **2011**, *6*, 97−104.
(13) Kisailus, D.; Choi, J. H.; Weaver, J. C.; Yang, W.; Morse, D. E. *Adv. Mater.* **2005**, *17*, 314−318.
(14) Cha, J. N.; Stucky, G. A.; Morse, D. E.; Deming, T. E. *Nature* **2000**, *403*, 289−292.
(15) Sumerel, J. L.; Yang, W.; Kisailus, D.; Weaver, J.; Choi, J. H.; Morse, D. E. *Chem. Mater.* **2003**, *15*, 4804−4809.
(16) Mueller, W. E. G.; Wang, X. H.; Kropf, K.; Ushijima, H.; Geurtsen, W.; Eckert, C.; Tahir, M. N.; Tremel, W; Boreiko, A.; Schlossmacher, U.; Li, J.; Schroeder, H. C. *J. Struct. Biol.* **2008**, *161*, 188−203.
(17) (a) Jovilet, J. P. *Metal Oxide Chemistry and Synthesis.: From Solution to Solid State*; Wiley & Sons: New York, 2000. (b) Ovenstone, J.; Yanagisawa, K. *Chem. Mater.* **1999**, *11*, 2770−2774. (c) Roy, R.; Hill, V. G.; Osborn, E. F. *J. Am. Chem. Soc.* **1952**, *74*, 719−722.
(18) Murr, M. M.; Morse, D. E. *Proc. Natl. Acad. Sci. U.S.A.* **2005**, *102*, 11657−11662.
(19) Schröder, H. C.; Boreiko, A.; Korzhev, M.; Krasko, A.; Tahir, M. N.; Tremel, W.; Eckert, C.; Müller, I. M.; Müller., W. E.G. *J. Biol. Chem.* **2006**, *281*, 12001−12009.
(20) Tahir, M. N.; Théato, P.; Müller, W. E. G.; Schröder, H. C.; Janshoff, A.; Zhang, J.; Huth, J.; Tremel, W. *Chem. Commun.* **2004**, 2848−2849.
(21) Kisailus, D.; Najarian, M.; Weaver, J. C.; Morse, D. E. *Adv. Mater.* **2005**, *17*, 1234−1239.
(22) André, R.; Tahir, M. N.; Link, T.; Jochum, F. D.; Kolb, U.; Theato, P.; Berger, R.; Wiens, M.; Schröder, H. C.; Müller, W. E. G.; Tremel, W. *Langmuir* **2011**, *27*, 5664−5671.
(23) Falabretti, B.; Robertson, J. *J. Appl. Phys.* **2007**, *102*, 123703/1−5.
(24) (a) Yang, F.; Forrest, S. R. *Adv. Mater.* **2006**, *18*, 2018−2022. (b) Snaith, H. J.; Ducati, C. *Nano Lett.* **2010**, *10*, 1259−1265.
(25) (a) Belliard, F.; Connor, P. A.; Irvine, J. T. S. *Solid State Ionics* **2000**, *134*, 163−167. (b) Meduri, P.; Pendyala, C.; Kumar, V.; Sumanasekera, G. U.; Sunkara, M. K. *Nano Lett.* **2009**, *9*, 612−616.
(26) Croft, G.; Fuller, M. J. *Nature* **1977**, *269*, 585−586.
(27) (a) Leite, E. R.; Weber, I. T.; Longo, E.; Varela, J. A. *Adv. Mater.* **2000**, *12*, 965−968. (b) Miller, T. A.; Bakrania, S. D.; Perez, C; Wooldridge, M. S. *Functional Nanomaterials: Nanostructured Tin Oxide Materials for Gas Sensor Applications*; American Scientific Publishers: Valenica, CA, 2006.
(28) Vollath, D. *Nanomaterials*; Wiley-VCH: Weinheim, Germany, 2008.
(29) Dai, Z. R.; Pan, Z. W.; Wang, Z. L. *J. Am. Chem. Soc.* **2002**, *124*, 8673−8680.
(30) Yang, R.; Wang, Z. L. *J. Am. Chem. Soc.* **2006**, *128*, 1466−1473.
(31) (a) Chen, B.; Russell, J. M.; Shi, W.; Zhang, L.; Samuiski, E. T. *J. Am. Chem. Soc.* **2004**, *126*, 5972−5973. (b) Vayssieres, L.; Graetzel, M. *Angew. Chem., Int. Ed.* **2004**, *43*, 3666−3770.
(32) Lin, Y.; Dong, J.; Liu, M. *Adv. Mater.* **2004**, *16*, 353−359.
(33) Zhang, D.-F.; Sun, L.-D.; Yin, J.-L.; Yan, C.-H. *Adv. Mater.* **2003**, *15*, 1022−1025.
(34) Birkel, A.; Reuter, F.; Koll, D.; Frank, S.; Branscheid, R.; Panthöfer, M.; Rentschler, E.; Tremel, W. *Cryst. Eng. Commun.* **2011**, *13*, 2487−2493.
(35) Yang, H. G.; Zeng, H. C. *Angew. Chem., Int. Ed.* **2004**, *43*, 5930−5933.
(36) Wu, S.; Cao, H.; Yin, S.; Liu, X.; Zhang, X. *J. Phys. Chem. C* **2009**, *113*, 17893−17898.
(37) Wiens, M.; Bausen, M.; Natalio, F.; Link, T.; Schloßmacher, U.; Müller, W. E. G. *Biomaterials* **2009**, *30*, 1648−1656.
(38) Chevalier, S.; Ayllon, C. C.; Grazu, V.; Luna, M.; Feracci, H; Fuente, J. M. *Langmuir* **2010**, *26*, 14707−14715.
(39) *EVAPlus Software Suite*; Bruker AXS: Madison, WI, 2010.
(40) Sauerbrey, G. *Z. Phys.* **1959**, *155*, 206−222.
(41) Roman, L. S.; Valaski, R.; Canestraro, C. D.; Magalhães, E. C. S.; Persson, C.; Ahuja, R.; da Silva, E. F. Jr.; Pepe, I.; Ferreira da Silva, A. *Appl. Surf. Sci.* **2006**, *252*, 5361−5364.
(42) Müller, W. E. G.; Rothenberger, M.; Borejko, A.; Tremel, W.; Reiber, A.; Schröder, H. C. *Cell Tissue Res.* **2005**, *321*, 285−297.
(43) Cölfen, H.; Antonietti, M. *Mesocrystals and Nonclassical Crystallization: New Self-assembled Structures*; Wiley-VCH, Weinheim, Germany, 2008.
(44) (a) Prime, K. L.; Whitesides, G. M. *Science* **1991**, *252*, 1164−1167. (b) Willner, I.; E. Katz, E. *Angew. Chem., Int. Ed.* **2000**, *38*, 1180−1218.
(45) Chevalier, S.; Ayllon, C. C.; Grazu, V.; Luna, M.; Feracci, H; Fuente, J. M. *Langmuir* **2010**, *26*, 14707−14715.